Granular Matter (2024) 26:70
https://doi.org/10.1007/s10035-024-01441-3

ORIGINAL REPORT

Effect of flexible membrane in triaxial test on the mechanical behaviour of rockfill material using Discrete Element Method

Reza Asadi[1,3] · **Mahdi M. Disfani**[1] · **Behrooz Ghahreman-Nejad**[1,3] · **Matteo O. Ciantia**[2]

Received: 12 November 2023 / Accepted: 18 May 2024

Abstract
The investigation of rockfill materials poses challenges due to their large particle size, associated high cost, and long laboratory testing duration. As a result, empirical correlations based on historical experimental studies are commonly used to design and analyse rockfill structures. However, the extensive use of rockfill in a wide range of applications and limited understanding of its mechanical behaviour emphasize the need for further research. These make it necessary to develop a robust technique capable of capturing key parameters such as particle shape and breakage, allowing for the simulation and study of large-scale assemblies with realistic boundary conditions. Given that the behaviour of rockfill is highly scale-dependent, primarily due to particle breakage, the simplified laboratory tests on the scaled-down assemblies can be misleading. Particle breakage is a fundamental phenomenon in the mechanical behaviour of rockfill and significantly affects shear strength, deformability, and porosity under different stress levels. The particle breakage is influenced by factors such as the rockfill's maximum particle size, mineralogy, particle shape, gradation, and confining stresses. This study adopts a computationally efficient breakage method called the Modified Particle Replacement Method (MPRM) based on the Discrete Element Method. A Tile-Based Flexible Membrane (TBFM) for triaxial test modelling has been developed by employing segmental rectangular walls to create a deformable membrane. The effects of critical parameters, including particle shape, confining stress, membrane resolution, degree of flexibility, and the characteristic strength of the particles, are examined. The findings of the combined MPRM-TBFM approach demonstrate the significant influence of membrane flexibility on volumetric-related behaviour.

Keywords Rockfill · Particle breakage · Discrete element method (DEM) · Large-scale triaxial test · Flexible membrane · Particle replacement method

1 Introduction

Rockfill is a widely used construction material in a range of geotechnical applications such as embankment dams, railway subgrades, and offshore structures. It comprises an assembly of rock aggregates ranging in size from less than 1 cm to over 1 m, typically falling within the range of 10 cm to 80 cm. Despite its extensive use, the current understanding of the mechanical behaviour of rockfill and its influential parameters still needs to be improved. Due to their large particle sizes, conducting laboratory tests on rockfill materials is challenging and resource-intensive. As a result, the design methods and analysis of rockfill structures heavily rely on a limited number of historical large-scale experimental studies [1, 2].

Several studies have employed a parallel particle size grading technique to address the scarcity of large-scale triaxial testing machines worldwide [3–5]. This technique involves testing and analysing a downscaled assembly of rockfill particles that exhibit a parallel particle size distribution (PSD) similar to the actual rockfill PSD. However, it is essential to note that the applicability of the parallel grading technique may be limited, as the behaviour of rockfill is significantly influenced by scale, primarily due to rock particle breakage [3, 6]. Consequently, there is a need to develop alternative analysis techniques that effectively account for essential parameters, such as particle shape and breakage, to comprehend rockfill's mechanical behaviour better.

✉ Mahdi M. Disfani
mmiri@unimelb.edu.au

[1] Department of Infrastructure Engineering, The University of Melbourne, VIC, Australia

[2] School of Science and Engineering, University of Dundee, Dundee, Scotland, UK

[3] ATC Williams Pty. Ltd., Melbourne, Australia

Published online: 05 June 2024

Particle breakage is a fundamental phenomenon that significantly impacts the shear strength, deformability and porosity, among other characteristics of rockfill under different stress conditions [2, 6, 7]. Particle breakage is influenced by various factors, including rock mineralogy, particle shape, surface roughness, particle size distribution, and confining stresses, albeit to different extents [8, 9]. Substantial settlements exceeding 1% of the dam height in rockfill dams often arise from rock particle breakage and rearrangement [10]. The breakage process leads to changes in the void ratio and PSD of the rockfill, which can be quantitatively assessed using the Relative Breakage Index (B_r) [11]. It is understood that particle breakage exerts a more pronounced impact on angular particles' shear strength than rounded particles. This phenomenon primarily arises from substantial alterations in the contact points of angular particles during breakage and a heightened probability of asperity breakage within angular particles. In the case of rounded particles, larger rock particles enhance interlocking and shear strength, while in the case of angular particles, particle breakage becomes more prominent with larger particle sizes [12]. The investigation of particle breakage in granular material, especially in the context of rockfill where breakage plays a significant role, has been explored through various methods, including single particle crushing [13] and X-ray tomography [14], as well as laboratory tests such as oedometer [15] and triaxial tests [16, 17]. However, most experimental studies have primarily focused on the characterization of particle breakage and related parameters at the end of testing [18]. On the other hand, numerical methods have provided researchers with the means to explore the evolution of breakage and its impact on the mechanical behaviour of rock particle assemblies.

DEM has gained significant popularity for investigating the behaviour of granular materials. This method involves simulating individual particles that interact with each other through equations of motion. The unique capability of DEM to capture intricate interactions among discrete elements makes it particularly suitable for modelling granular materials, including rockfill. In DEM modelling, various particle shapes can be represented, ranging from spherical and elliptical to more complex angular assemblies such as overlapped configurations like Fourier-based shapes [19] and bonded non-overlapped sub-particles. Figure 1(a) provides visual examples of bonded non-overlapped spherical sub-particles to generate angular shapes. To simulate more intricate shapes, computational efficiency may be compromised by employing numerous finer sub-particles. Several techniques have been introduced within DEM to simulate particle breakage. For instance, coupled DEM with Finite Element Methods (FEM) can accurately capture breakage surfaces by integrating DEM and FEM [20, 21]. In this coupled approach, the interactions between particles are modelled using DEM, while individual particles are discretised and analysed using FEM.

A more computationally efficient approach involves the use of bonded particles, where particle breakage is modelled by altering the bond strength between sub-particles [22]. In this method, each mother (original) particle is represented by bonded sub-particles. While the simulation of granular assemblies using bonded particles is faster compared to the coupled DEM-FEM approach, it still requires significant computational resources when modelling assemblies of a reasonable size. Although these methods provide a

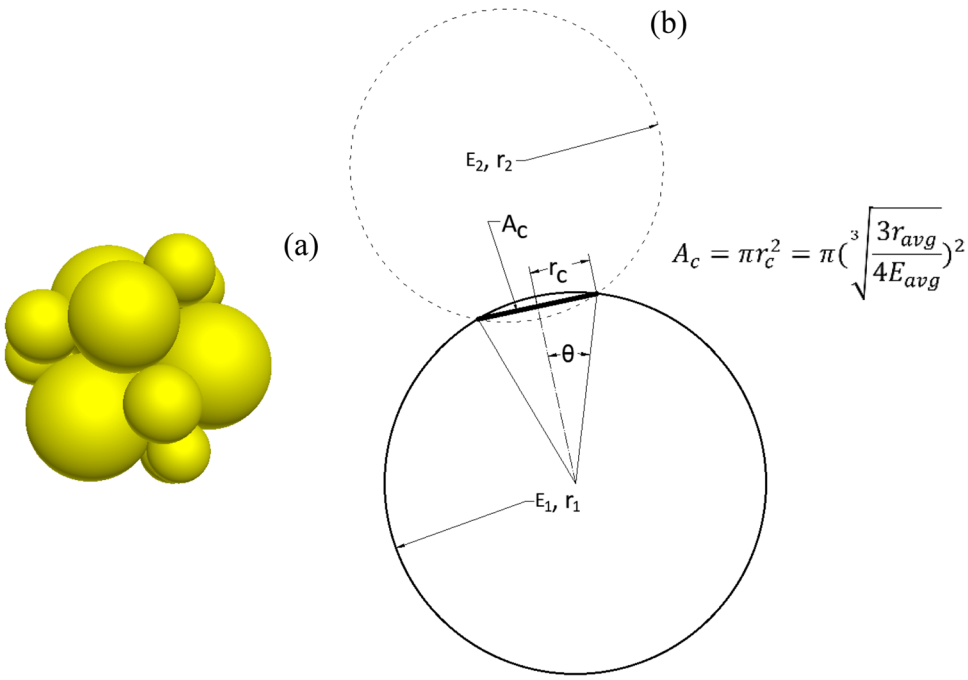

Fig. 1 Illustration of angular particle geometry using **a**) bonded non-overlapped sub-particles, along with **b**) contact geometry based on Hertzian theory

comprehensive understanding of the micro-mechanics of particle breakage [23], alternative techniques have been proposed to balance accuracy and computational demand. One such technique is the particle replacement method [24, 25], which offers improved computational efficiency while maintaining acceptable accuracy. In the replacement method, a broken particle is identified based on specific breakage criteria [26, 27] and replaced by an assembly of finer particles. Typically, the particles in this method are simulated as spherical or circular elements. A more sophisticated model can be developed by considering different breakage patterns and particle sizes for the newly introduced smaller particles, considering the mother particle's stress conditions [28]. However, there are two critical aspects of the replacement method that require further improvement: (i) the representation of the shape of the mother particle and (ii) accounting for the mass loss resulting from the replacement of the mother particle by an assembly of daughter particles with a smaller volume (mass). To address these aspects, an advanced replacement method is introduced [29] to investigate the mechanical behaviour of rockfill materials.

Element testing with DEM has traditionally relied on periodic boundaries or rigid frictionless walls [30]. However, in specific scenarios, such as testing highly breakable materials, determining clay strength, and when studying the shear band zones, particularly for rockfill and other coarse-grain materials, results are significantly influenced by boundary conditions, deformable membranes, and shear localization, as observed in this study. To tackle these challenges, this research adopts a model capable of integrating physical boundaries, allowing for the simulation of realistic boundary conditions and the investigation of deformable membrane behaviour. This approach markedly enhances the accuracy and applicability of the simulations in situations where traditional boundary conditions fall short.

Two techniques are commonly employed to simulate the physical boundary condition and membrane using DEM: (i) the assembly of spheres/balls surrounding the sample, and (ii) the use of rigid walls, which is the more prevalent approach. In the first technique, bonded marginal particles can be placed at the perimeter of the sample and treated as a membrane during the simulation. Alternatively, the marginal particles can be considered as the membrane without any bond in each simulation cycle. However, when using the unbonded marginal element method, the boundary particles may shift into a loose assembly, decreasing computational efficiency as the search for peripheral elements becomes more challenging in each cycle. Although efforts have been made to develop strategies for calibrating microparameters, particularly those related to bonded particles [31], the model can be further improved by addressing the following factors: (i) calibration of membrane bonds under different stress conditions, particle sizes, and shapes; (ii) necessary adjustments to the bonded particles to account for large deformations; and (iii) incorporation of a sufficient number of marginal particles to accurately capture the performance of the membrane [32]. Consequently, the use of rigid walls has become the most common boundary condition in DEM modelling, often taking the form of a semi-rigid, frictionless [33] cylinder acting as the membrane in triaxial and other element test simulations.

In the context of triaxial test modelling, a cylindrical wall constructed from rectangular platens can be employed, with the number of platens varying depending on the desired resolution. This approach ensures symmetrical consolidation of the sample and prevents local bulging. Liu et al. [34] conducted a study on the impact of resolution in segmenting the cylindrical wall into rigid vertical segments and deformable articulated wall segments composed of triangular parts, focusing on rockfill's compaction and mechanical behaviour. Another option is to segment the wall horizontally into small cylindrical rings, as proposed by Zhao & Evans [35], to achieve a flexible boundary. However, in this method, the sample experiences symmetric confinement in the diagonal direction, as the independent rings can contract or expand while their centroid remains fixed. To combine the simplicity and computational efficiency of a rigid wall with a fully deformable membrane in all directions, a hybrid approach involving both horizontal and vertical segmentation, known as tile theory, has been suggested by Khoubani & Evans [36].

In this study, the authors investigate the mechanical behaviour of rockfill using the Modified Replacement Method [29], an algorithm previously introduced by the authors for simulating particle breakage. Additionally, the effect of a flexible boundary on particle breakage and mechanical behaviour is explored through the application of tile theory, where independent small rigid rectangular walls are utilised to form a cylindrical deformable membrane that can freely move inward and outward to achieve the desired confining stress. To streamline the investigation of deformable boundaries, an idealized prototype of uniform particle size using rockfill material in this study is developed. The objective is to comprehend the impact of boundary conditions on particle breakage and the behaviour of rockfill material, thereby laying the groundwork for more advanced and realistic rockfill modelling.

2 Numerical modelling

2.1 Modified particle replacement method (MPRM)

The modified particle replacement method can efficiently capture the particle breakage phenomenon. The details of this method are presented and discussed in another publication [29]. DEM-based methods that utilise the traditional particle replacement mechanism often employ circular or

spherical shapes for computational efficiency and later replace them with a finer assembly of sub-particles following breakage. The MPRM model differs from other methods due to its ability to simulate particle shape, which has yet to be considered by others. Any particle shape is simulated using non-overlapped spherical particles and Apollonian packings, which is one of the advantages of this method. The second key advantage of this method is its computational efficiency, achieved by modelling the particles as rigid clumps from the outset. Due to the rigidity of the clump particles, the computational demand is significantly reduced since there is no need to analyse internal contacts between sub-particles. This advantage becomes evident when contrasting rigid clumps with bonded assemblies of particles, where numerous bonds must be examined for potential breakage in each simulation cycle [37]. Throughout the simulation, the maximum contact force of each particle is monitored at specified intervals. Using the maximum contact force as the breakage criterion has been proven to capture the macroscopic behaviour in particle breakage accurately. Additionally, it effectively accounts for the continuous breakage of smaller daughter particles and generates coherent, normally consolidated lines and fractal PSDs in alignment with experimental data [27]. Several breakage criteria have been proposed and utilised in DEM simulations for studying particle breakage, such as; (i) Octahedral shear stress, (ii) Mean particle stress, (iii) Major principal stress, (iv) Particle stress derived from the maximum contacts force and its diameter $\left(\sigma = {}^{F_{max}}\!/_{d^2}\right)$ [27], (v) Particle characteristic strength which is derived from the tensile and compressive properties of the particle and applied as a limit stress to the contact stress of particles calculated based on Hertzian contact theory [38].

De Bono and McDowell [27] evaluated the criteria mentioned above through DEM simulation of one-dimensional consolidation tests. As previously mentioned, different studies [27, 38, 39] have demonstrated that the maximum contact force criterion exhibited significant compatibility with experimental results and observed behaviour. The maximum contact force at breakage (F_{max}) can be derived from the particle's characteristic strength ($\sigma_{0|d_0}$) at the reference diameter (d_0) as shown in Eq. 1.

$$F_{max} = \left[\sigma_{0|d_0} \times \left(\frac{d}{d_0}\right)^{-3/m} \times \pi \left(\frac{3r_{avg}}{4E_{avg}}\right)^{2/3}\right]^3 \quad (1)$$

where the contact area (illustrated in Fig. 1(b)) is calculated using the average contact radius (r_{avg}) and average modulus of elasticity (E_{avg}), and the characteristic strength may be scaled for different particle sizes using Weibull's modulus [40]. The characteristic strength of particles can be evaluated using the compressive (σ^c) and tensile (σ^t) strengths of the particle [26]. Utilizing this method and equation, the experimental tests conducted on a reference particle with a diameter of d_0 facilitate the derivation of the reference characteristic strength ($\sigma_{0|d_0}$). Subsequently, this reference strength can be extrapolated for various particle sizes by employing a scaling factor of $\left(\frac{d}{d_0}\right)^{-3/m}$ [41], accounting for the statistical strength distribution based on the Weibull modulus across different sizes. Ultimately, the scaled strength can be transformed into the maximum contact force by applying Hertzian theory, considering the average contact area between the interacting particles [23].

As shown in Fig. 2, during the simulation cycling, if an initial non-breakable particle (clump) is diagnosed in critical stress (i.e., 90% of its characteristic strength), it will be replaced by a cluster of bonded sub-particles (balls) of identical size occupying the same position. In this way, the model will only investigate the internal contacts of a particle that is near breakage, so the simulation will be fast and computationally efficient. The linear parallel bond method has been utilized to model the bonding between sub-particles of the substituted breakable particles. In a single particle crushing test, where the particle is compressed between two parallel platens, the bond parameters have been calibrated to ensure that the particle's strength at the point of breakage matches its characteristic strength. The mobilised stress of the particle is computed based on the contact force between the particle

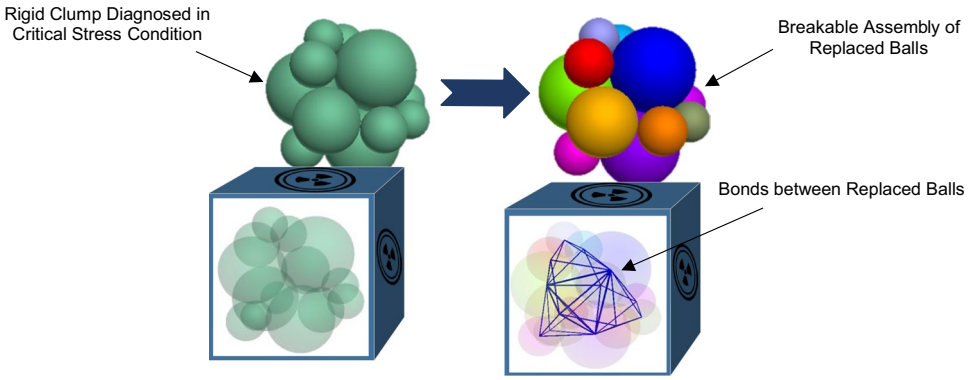

Fig. 2 Schematic illustration of Modified Particle Replacement Method

and the platens, and the particle's diameter [29]. In this test, a single particle, randomly oriented between two platens, is gradually compressed until it reaches its maximum strength and ultimately fractures. The parallel bond parameters are adjusted iteratively to achieve the desired characteristic strength, with calibration continuing until a variation of less than two percent from the target is attained. To validate this calibration procedure, the crushing tests will be repeated for the same number of tests as during calibration. The strength variation will be monitored to ensure it remains within the previously mentioned maximum allowable range. A detailed procedure for MPRM and parameter calibration is outlined in the authors' previous publication [29].

2.2 Tile-based flexible membrane (TBFM)

The deformable boundary conditions and flexible membrane in this study are simulated using a group of rectangular segments known as Tiles. ITASCA PFC^{3D} software has been used for the DEM simulation. The difficulties with; (i) calibration, and (ii) the limited confining pressure available through bonded circumferential individual elements (bonded ball particles) serving as a deformable boundary, render this method constrained and challenging to employ. Conversely, the presence of dissociated and independent walls in the PFC platform paves the way for the concept of TBFM, offering an optimum and novel approach for the simulation of the flexible membrane in triaxial testing.

The cylindrical flexible membrane in triaxial testing has been traditionally simulated using a semi-rigid membrane. As shown in Fig. 3(a), the membrane is divided into rectangular vertical strips (walls) which move forward and backward together to apply target confining stresses.

A fully flexible membrane can be achieved by a series of overlapped tiles generating rings around the sample. These rings together form a flexible cylinder, as illustrated in Fig. 3(b). In contrast to a semi-rigid cylinder in which all segments must move together, here, each tile can independently move forward or backward to reach any stress levels. Hence, bulging and block shearing of the sample can be adequately captured in this method. The top and bottom caps are simulated as a platen wall, as shown in Fig. 3(c).

The number of tiles and their size should be adjusted to create a balance between the computational demand and deformability of the membrane. The minimum dimension of a tile should also be larger than the smallest particle size so it remains in contact with the particles and the target confining stress could be calculated. Each tile is overlapped (Fig. 3(c)) with its neighbours in a ring of tiles so that no gap can form due to the backward movement of the tile. The number of stacked rings vertically should be enough to accurately capture the sample's volumetric deformation (bulging or shearing) of the assembly. The circular cross-section of the membrane can be estimated by different number of tiles in each ring (H_{part}). The area difference with the circumscribed circle for different numbers of tiles is illustrated in Fig. 3(d). It is clear that for $H_{part} > 20$, the area difference is below %1. Hence, in this study, the number of tiles in each ring is limited to 20 with different numbers of rings (V_{sec}) investigated. Furthermore, taking into account the stipulated minimum tile dimension necessary for maintaining contact with the particles, as previously discussed, Fig. 3(d) also illustrates the ratio of tile width to the uniform particle size of 2 cm in this study.

The servo program controls the stress condition of each tile independently, so considering the contact forces acting on each tile, it will move forward or backward to achieve a given stress level. Taking into account the lateral overlap of tiles to prevent horizontal gaps between them, a sub-program has been developed to determine the active area of each tile by considering its position and adjacent tiles. The loading rate and the velocity of tiles are limited in a way that the confining stress remains constant, and a quasi-static condition is attained. Hence, the maximum inertial number (I), as presented in Eq. 2, is limited to 10^{-4} which is strictly below the recommended value of 10^{-3} [36].

$$I = \frac{\dot{\varepsilon} \times d_{50}}{\sqrt{p'/\rho_s}} \tag{2}$$

where $\dot{\varepsilon}$ stands for strain rate, d_{50} is the average particle diameter, p' is the average mean effective stress across the sample, and ρ_s is the particle density.

Given that the walls in the PFC platform are two-dimensional without thickness, a significant difference in displacement between a pair of top and bottom walls could result in a gap large enough for particles to escape. Dividing the height of the cylinder into sufficiently small ring segments (i.e., increasing the number of vertical segments, denoted as V_{sec}) ensures a smoother stress distribution among all rings, thereby limiting the differential displacement between two adjacent vertical tiles. In essence, increasing the number of vertical segments (Vsec) serves as a means to mitigate substantial gaps between tile rings.

In addition to the strategy of limiting tile size to prevent the generation of gaps between vertically adjacent tiles, sub-programs have been integrated into the model to monitor and control vertical gaps. Within the gap-control sub-program, if a gap larger than the minimum particle size present in the assembly is detected, adjustments are made to the servo control program. These adjustments depend on the sign and direction of the velocities of the tiles between which the gap occurs. The positive direction is defined as toward the central axis of the cylindrical membrane, as illustrated in Fig. 4(a). The flowchart for the vertical gap control sub-program is depicted in Fig. 4(b).

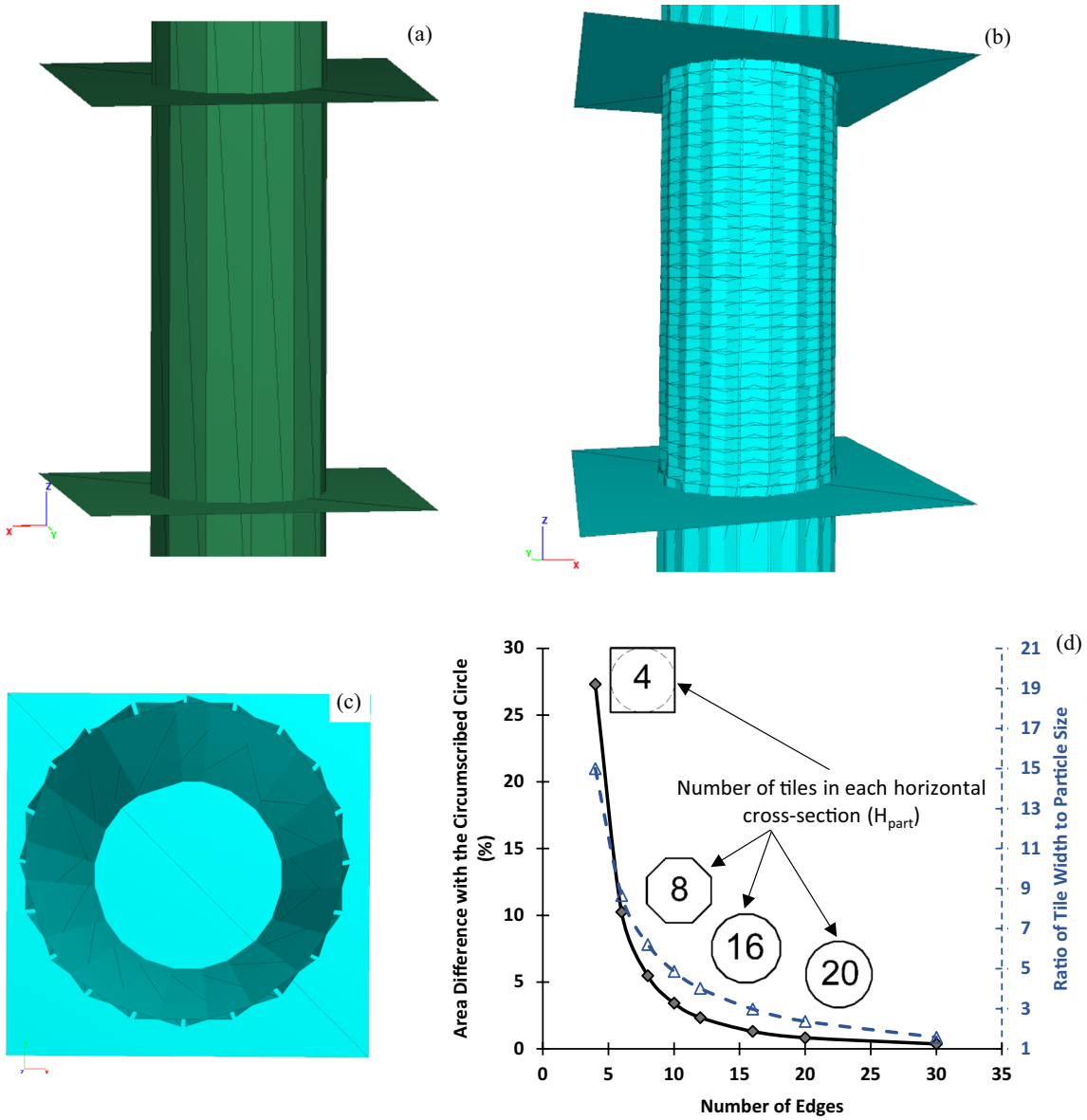

Fig. 3 Triaxial membrane model: a) Semi-rigid (Solid) vessel composed of vertical strips, b) Cylindrical membrane generated by independent rectangular tiles ($V_{sec}=36$), c) Plan view of the top platen and first row of overlapped tiles ($H_{part}=20$), d) Area difference with the circumscribed circle for different number of tiles

When a gap (g_n) opens between the n-th and (n + 1)-th tiles and reaches the minimum particle size, the velocity of tile (V_n) is adjusted to decrease the gap size below the minimum particle size. If both tiles are moving toward or away from the central axis (i.e., $sign(V_n)=sign(V_{n+1})$), the relative velocity is temporarily reduced to close the gap. However, if the tiles are moving away from each other (i.e., $sign(V_n)\neq sign(V_{n+1})$), the relaxing mechanism is triggered ($V_n=V_{n+1}=0$) to facilitate stress redistribution. If the newly calculated velocities based on the stresses following relaxation result in gap reduction, the walls become active once again.

Through the utilization of the gap-control sub-program alongside meticulous attention to tile sizing, the average confining stress experienced by the tiles exhibits a deviation of no more than 0.1% from the intended confining stress level. Consequently, the modelling can be extended to encompass significant axial and volumetric strains.

2.3 Triaxial testing simulations

For triaxial testing, the clumps are assembled in a larger vessel to ensure sufficient space for particle generation without overlap. The non-overlapping particles form a porous

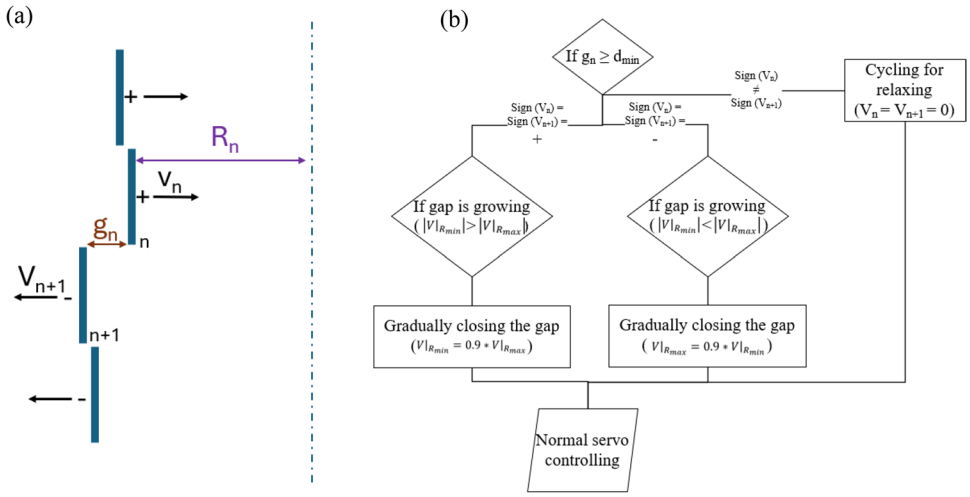

Fig. 4 Gap controlling system between vertically adjacent tiles; **a**) schematic illustration of vertically adjacent tiles and their velocities (V_n) and distance from the central axis of the cylinder (R_n); **b**) the flowchart for vertical gap control sub-program

cloud, which is then compressed to the final desired membrane size by moving the walls and particles towards the centre of the vessel. During this stage, the wall velocity is maintained at a very low level to prevent the generation of excessive velocity and stress in the particles. Once the target size is achieved and the particle assembly is compacted, the simulation proceeds without further wall movement, allowing the particles to reposition themselves and release any accumulated stresses and out-of-balance forces. The relaxation stage of the simulation persists until the maximum unbalanced force ratio falls below 0.1%, and the mean effective stress, which has been observed in three distinct spherical zones located at the top, middle, and bottom of the sample, becomes negligible, registering at less than 1 kPa.

During the compaction and shearing stage of triaxial modelling, the prepared sample from the previous stage is utilised. To achieve the desired confining stress for each triaxial model, the tiles independently adjust their positions and move towards or away from the central axis of the cylindrical membrane considering the target confining stress and current existing stress exerted by the particles in contact. Hence, the tiles are servo controlled based on the difference between the current and target confining pressure. To ensure the stability and consistency of the applied confining stress, the maximum allowable velocity of the tiles is set at a negligible value of 0.01 mm/s. This serves two main purposes: (i) preventing the application of excessive forces and stresses on the particles, and (ii) maintaining a constant and stable confining stress level, thereby preventing any fluctuations in the confining stress.

In this study, two different particle shapes composed of 14 and 4 balls have been employed as shown in Fig. 5(a) and (b), respectively. The sphericity index ($\Phi = A_e/A_p$), defined as the ratio of the surface area of a sphere with the same volume as the particle (A_e) to the surface area of the particle (A_p) [42], measures 0.86 for the 14-ball clump and 0.71 for the 4-ball clump. Therefore, as anticipated, the 4-ball clump exhibits less roundness and a more angular shape compared to the 14-ball particle. For the parametric study of the numerical model, a series of triaxial tests on cylindrical samples (30 cm diameter and 70 cm tall with a porosity of 58%) have been modelled. The adopted DEM parameters are listed in Table 1. The triaxial testing simulations have been conducted using semi-rigid and tile-based flexible membranes with $H_{part} = 20$, and $V_{sec} = 12$, 24, and 36 that account for 240, 480, and 720 tiles in total, respectively. The linear contact model is employed for the interaction of particles, with the parallel bonding adopted between the sub-particles of replaced critical particles.

The samples, prepared in accordance with the previously outlined procedure and measuring 30 cm by 70 cm, were employed for the triaxial modelling. It is worth noting that a uniform particle size of 2 cm is used in the parametric study. The target confining pressure is achieved by servo-controlled movement of the walls, and finally, the shearing load is applied by the top and bottom platens' strain-controlled movement. In addition to the inertial number criteria, the shearing rate and the velocity of all the walls are limited to a very slow rate so that the target confining stress is maintained at a constant level (tolerance < 0.1%) throughout the simulation.

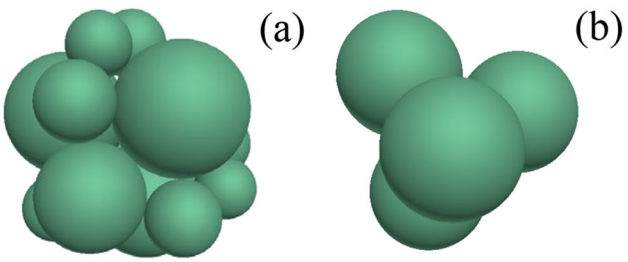

Fig. 5 Particle shapes employed for numerical simulations: **a**) 14 Balls, **b**) 4 Balls

Table 1 DEM parameters

Parameters	Value		
	Weak	Medium	Strong
Characteristic Strength of particle (MPa)	23.2	43.2	350.7
Linear Parallel Bond Tensile Strength (N/m^2)	0.3×10^8	0.5×10^8	4.2×10^8
Linear Parallel Bond Cohesion (N/m^2)	0.6×10^8	1.0×10^8	8.4×10^8
Young's Modulus, E (GPa)	46.8		
Poisson Ratio, ν	0.3		
Linear Normal Stiffness (N/m)	5.8×10^6		
Linear Shear Stiffness (N/m)	2.9×10^6		
Linear Parallel Bond Normal Stiffness (N/m)	9.6×10^8		
Linear Parallel Bond Shear Stiffness (N/m)	4.8×10^8		
Top/Bottom Platen Normal Stiffness (N/m)	3.2×10^8		
Tile Normal Stiffness (N/m)	3.2×10^6		
Coefficient of Friction	0.3		
Sample Initial Porosity	58%		

3 TBFM resolution

The number of tiles employed in the triaxial modelling has a direct impact on the membrane's flexibility and its ability to capture deformations. However, it is crucial to ensure that the minimum dimension (width) of the tiles remains larger than the minimum particle size. This guarantees that there is always a potential for contact between the tiles and particles, preventing the tiles from penetrating the inter-particle voids. Additionally, the dimensions of the tiles are determined to allow for a certain degree of overlap between adjacent tiles. This overlap ensures that as the tiles move towards or away from the cylinder axis, there is continuous overlap between them, eliminating any gaps that might allow particles to escape.

It is important to note that in the PFC^{3D} platform, the walls are represented as two-dimensional elements, assuming they have negligible and insignificant thickness. Consequently, the vertical overlap alone cannot prevent the generation of gaps between a given ring of tiles and the rings above and below it. To address this concern and prevent gap formation in the vertical direction, it is necessary to have a considerable number of vertical sections (rings), ensuring that the difference in tile displacement remains smaller than the minimum particle size. This effectively renders any generated gaps negligible. In other words, the number of vertical segments and tile rings should be large enough to ensure a gradual change in stress conditions between two consecutive rows, minimizing the gradient of displacement and ensuring that any generated gaps remain substantially smaller than the minimum particle size. However, it is important to consider that increasing the number of tiles leads to a substantial logarithmic increase in simulation time, as well as an elevated computational demand. Consequently, the selection of the number of tiles should strike a balance between meeting deformation modelling requirements, minimizing gap formation, and maintaining computational efficiency within acceptable and practical limits.

Figure 6 presents the results of the triaxial test performed on a 14-ball-shaped rock particle sample using a flexible membrane with varying numbers of tile rows (V_{sec}) and solid (semi-rigid) membrane under a confining stress of 2 MPa. In these models, each row/ring consists of 20 tiles (H_{part}), and the impact of tile resolution is investigated using 36, 24, and 12 rows of tile rings. The behavioural trends and outcomes observed in these triaxial tests on breakable particles align with other researchers' findings [43, 44]. The difference in the anticipated stress–strain behaviour between the flexible and solid membranes is comparatively negligible for the sample with stronger particles, but it becomes more conspicuous in the case of weak particles, where notable particle breakage is evident. For assemblies containing Medium to Strong particles with limited breakage, as shown in Fig. 6(a) and (b), the predicted deviatoric stress in the solid vessel is slightly higher than that in the flexible membrane. However, in the case of weak particles where breakage is more prevalent (as shown in Fig. 6(c)), the analyses using flexible membranes demonstrate higher peak and residual strengths. The residual strength is primarily associated with the state of deviatoric stress after reaching the peak stress, also for axial strains exceeding 20%. Therefore, it can be inferred that the utilisation of a flexible membrane facilitates the rearrangement of particles and leads to the generation of higher strength. Moreover, as the resolution of tiles and flexibility of the membrane increase, the stress-related behaviour of the sample transitions from a dense to a loose-type behaviour. Instead of reaching a peak strength and subsequently dropping to an almost constant deviatoric stress, the strength

exhibits an increase to the peak and gradually demonstrates continuous decrease within the residual zone.

When it comes to impact of using TBFM method on volumetric response, the volumetric strain diagrams indicate that samples confined by the semi-rigid or solid membrane display a more dilative behaviour. Furthermore, even weak particles (Fig. 6(c)) exhibit less contraction when tested with the solid membrane compared to the flexible membrane. This can be attributed to the restricted longitudinal movement and lack of bending flexibility of the semi-rigid membrane, along with the strain localization in the middle of the samples. In other words, when shear bands form in the middle of the sample and exert high pressure on the membrane, the entire membrane resists dilation to maintain constant confining stress. Consequently, the entire sample demonstrates a noticeable apparent dilative behaviour. The influence of membrane flexibility and deformable boundary conditions on the volumetric behaviour and deformation of samples is evident. While transitioning from a semi-rigid or solid vessel to flexible membranes leads to a considerable reduction in dilation, an increase in the number of tile rings and resolution results in a rebound of dilation and a shift towards positive volumetric strains. Finally, it can be concluded that the (20 × 36) tile arrangement produces the highest accuracy for the simulation of the breakable rockfill particles.

To investigate the impact of confining stress along with the effect of tile resolution on the mechanical behaviour of breakable particles, i.e. Weak and Medium particles, a reduced confining stress of 1.5 MPa was examined, as depicted in Fig. 7. Some differences in the mobilized deviatoric stress for the medium-strength assemblies (Fig. 7 (a)) between the solid wall and flexible (36-row tiles) membranes are observed after the initial stage of shearing and prior to converging at residual stress levels. The variation in volumetric behaviour followed a similar pattern to that of 2 MPa confining stress for medium-strength assemblies in which the solid membrane has resulted in a significant degree of dilation, compared to larger contractions for samples with a flexible membrane. Additionally, at lower tile resolution (Tile 24), increased breakage led to greater contraction, while higher tile resolution (Tile 36) produced a smoother stress distribution that prompted particle rearrangement and resulted in slightly higher levels of dilation. Taking into account the findings for less breakable particle assemblies, namely medium and strong particles under both 1.5 and 2 MPa confining stresses, the lower tile resolution may result in delayed deviatoric stress mobilization and hence the peak strength is reached at higher axial strains.

The significant, continuous particle breakage, followed by the rearrangement of broken particles, leads to the observed fluctuations in deviatoric stress and volumetric strain in Fig. 7(b) with 24 rows of tiles (representing a weak assembly). The relationship between the development of axial deviatoric stress and the increasing number of fractures is also depicted in Fig. 7(b). This diagram reveals a distinct surge in fracture events for a lower membrane resolution of Tile 24, coinciding with a decrease and fluctuation in its deviatoric stress diagram. Conversely, the increment of fractures for a higher resolution of Tile 36 progresses smoothly, resulting in minimal fluctuation observed in the deviatoric stress diagram for this assembly. Consequently, it becomes evident that for weak and highly breakable particles, the mechanical response of the assembly is exceptionally sensitive to both membrane flexibility and tile resolution. Figure 7(b) highlights a clear example of this sensitivity. Similar to weak samples subjected to 2 MPa stress (Fig. 6(c)), for samples with 1.5 MPa confining stress, the tiled membrane (Tile 36) exhibits higher deviatoric stress, while the dilation captured within the semi-rigid or solid membrane consistently exceeds that observed in the tiled membrane. The trends of fluctuations in deviatoric stress and volumetric strain across varying confining stresses and for different characteristic strengths exhibit strong compatibility and agreement with the results reported in numerical modelling [45] and experimental investigations [18, 46] of triaxial testing for rockfill material.

A clearer understanding of how membrane deformability affects particle breakage and stress localization can be gained through Fig. 8. This figure illustrates the development of fractures with increasing axial strain for weak particles in both Tile 24 and Tile 36 membranes. It is evident that with lower membrane resolution, particle breakage events primarily occur near the top and bottom platens, resulting in a significantly higher number of fractures compared to the higher resolution membrane.

The distribution of fractures and breakage events within the cross-section of the triaxial sample, along with their respective magnitudes, can provide insight into the variations in the breakage phenomenon and its impact on the mechanical behaviour of the assemblies. * MERGEFORMAT Fig. 9 illustrates the fracture rosette diagram for the cross-section of triaxial cylindrical cells with different tile resolutions under confining stress of 2 MPa, at residual and post-peak strains. These rosette diagrams illustrate the average frequency of breakage events and their associated directions along the cylindrical triaxial sample.

In the case of medium particles with limited breakage events, increasing the membrane resolution generally leads to a smoother distribution of fractures in all directions. This is evident when comparing Fig. 9(a) for the solid membrane with Fig. 9(c) and (d) for 24 and 36 rows of tiles, respectively. However, the quantity of fractures and the number of breakage events exhibit no discernible pattern and show fluctuations with an increase in tile resolution. For medium particles, which exhibit greater strength compared to weak

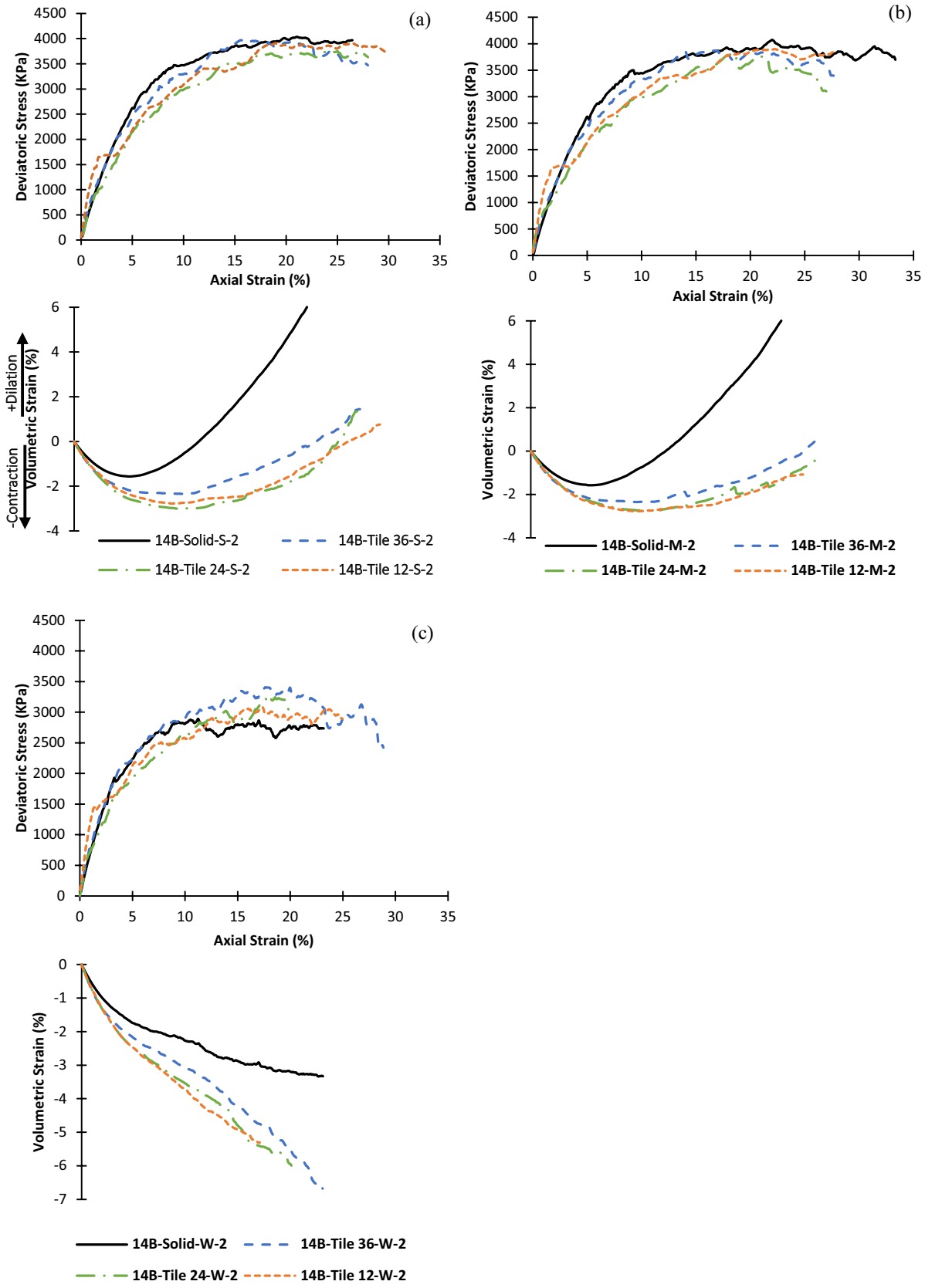
(a)
Deviatoric Stress (KPa)
Axial Strain (%)
+Dilation
-Contraction
Volumetric Strain (%)
14B-Solid-S-2
14B-Tile 36-S-2
14B-Tile 24-S-2
14B-Tile 12-S-2
(b)
Deviatoric Stress (KPa)
Axial Strain (%)
Volumetric Strain (%)
14B-Solid-M-2
14B-Tile 36-M-2
14B-Tile 24-M-2
14B-Tile 12-M-2
(c)
Deviatoric Stress (KPa)
Axial Strain (%)
Volumetric Strain (%)
14B-Solid-W-2
14B-Tile 36-W-2
14B-Tile 24-W-2
14B-Tile 12-W-2

◂**Fig. 6** Numerical triaxial test results for different number of tiles' rows (V_{sec}) and solid (semi-rigid) vessel for 2 MPa confining stress and **a**) Strong, **b**) Medium, and **c**) Weak particles. (The shortened titles in the legend indicate: Particle shape-Solid or Tiled (including resolution) – Particle strength – Confining stress in MPa)

ones, stress redistribution primarily occurs through the relocation and rearrangement of particles. A slight increase in flexibility, as seen when transitioning from Solid to Tile 12 (i.e. Figure 9(a) to (b)), results in a slightly smoother movement of the particles, leading to a slight reduction in the number of fractures. However, it is important to note that the central region of the sample, where most particle shifting and translation occur, is confined by a limited number of tile rings. Considering that particle breakage tends to concentrate in zones with a high gradient of relative particle translation, a significant increase in flexibility and the addition of more tile rings offer the potential for the creation of zones with a high gradient of relative translation, resulting in an increase in fracture events. This is evident when comparing Fig. 9(a) and (b) with Fig. 9(c). Conversely, a further increase in flexibility and transitioning from 24 to 36 rows of tiles leads to smoother stress distribution and relative displacement between two successive rows of tiles. Consequently, this results in a slight decrease in the amount of breakage, as observed when comparing Fig. 9(c) and (d).

As anticipated, the fractures demonstrate a more uniform distribution across all directions in the case of weak particles, characterized by their high susceptibility to breakage. Augmenting the membrane resolution by incorporating a greater number of tile rows yields an escalated occurrence of fractures in all directions, as vividly illustrated in Fig. 9(f) to (h) (note that the graphs are not to scale, and the quantity of fractures varies in each graph e.g., the fractures increase from 1131 to 1490 between Fig. 9(f) and (h)). This elevated number of breakages facilitates an improved reorganization of particles, consequently resulting in slightly heightened deviatoric stresses within the membrane of Tile 36, shown in Fig. 6(c).

The impact of confining stress on fracture distribution can be analysed through a comparison of the findings depicted in * MERGEFORMAT Fig. 10, which illustrates the fracture results under a lower confining stress of 1.5 MPa, with the previously discussed fracture diagrams obtained under a confinement of 2 MPa. When examining relatively lower confining stresses for medium-strength particles, transitioning from a semi-rigid membrane (Fig. 10(a)) to a tile-based membrane with a resolution of 24 (Fig. 10(b)) leads to a higher number of broken particles but a smoother distribution in all directions. This trend is reversed when the resolution is increased to 36, wherein the frequency of fracture events decreases while the variation in different directions increases, as evident in Fig. 10(c). The trends observed for medium particles remain consistent even with the higher confining stress of 2 MPa, and these trends are attributed to the variations in zones with different gradients of relative translation mentioned earlier. In the case of weak particles and highly breakable materials, employing a flexible membrane and increasing resolution and flexibility generally results in a reduction of fracture events in all directions. Additionally, a flexible membrane and higher resolution compromise the smoothness of the fracture rosette, leading to a fluctuating fracture distribution, as obvious in Fig. 10(f). Comparing the fracture distribution among weak particles subjected to low and high confining stresses (i.e., 1.5 and 2 MPa) through Figs. 10 and 9 reveals that an increase in flexibility and the number of tile rows leads to a smoother stress redistribution under relatively low confinement (1.5 MPa), resulting in a decrease in fracture events. It is important to note that under low confining stresses, particle rearrangement facilitates stress redistribution, and increased flexibility aids in this rearrangement, preventing breakage. Conversely, at relatively high confining stresses of 2 MPa, achieving significant confinement requires substantial displacement of tile walls, leading to a higher incidence of particle breakage. In other words, under relatively high confining stresses, particle breakage becomes the primary mechanism for stress redistribution. Consequently, an increase in the number of tile rows results in a higher occurrence of fracture events.

4 Particle shape effect

As previously stated, MPRM offers the advantage of incorporating particle shape in the modelling process with optimal computational efficiency from the beginning of modelling. To examine the stress–strain behaviour of samples comprised of various particle shapes, Fig. 11 presents the results of triaxial modelling using two distinct particle shapes composed of 14 and 4 balls (shown in Fig. 5(a) and b)) at two different confining stresses of 1.5 MPa and 2 MPa, using uniform particle sizes of 2 cm.

It is evident from the comparison of Figs. 6 and 11 that the difference in mobilised deviatoric stress between the solid and flexible membranes is lower for particle shape 4B than for particle shape 14B, particularly when considering the weak particles (Figs. 6(c) and 11(c)). However, the trend in volumetric behaviour for both shapes is almost identical. The assembly of 4B particles shows a higher strength in comparison to that of 14B particles due to higher angularity. This distinction becomes more pronounced in the case of weak particles for both semi-rigid

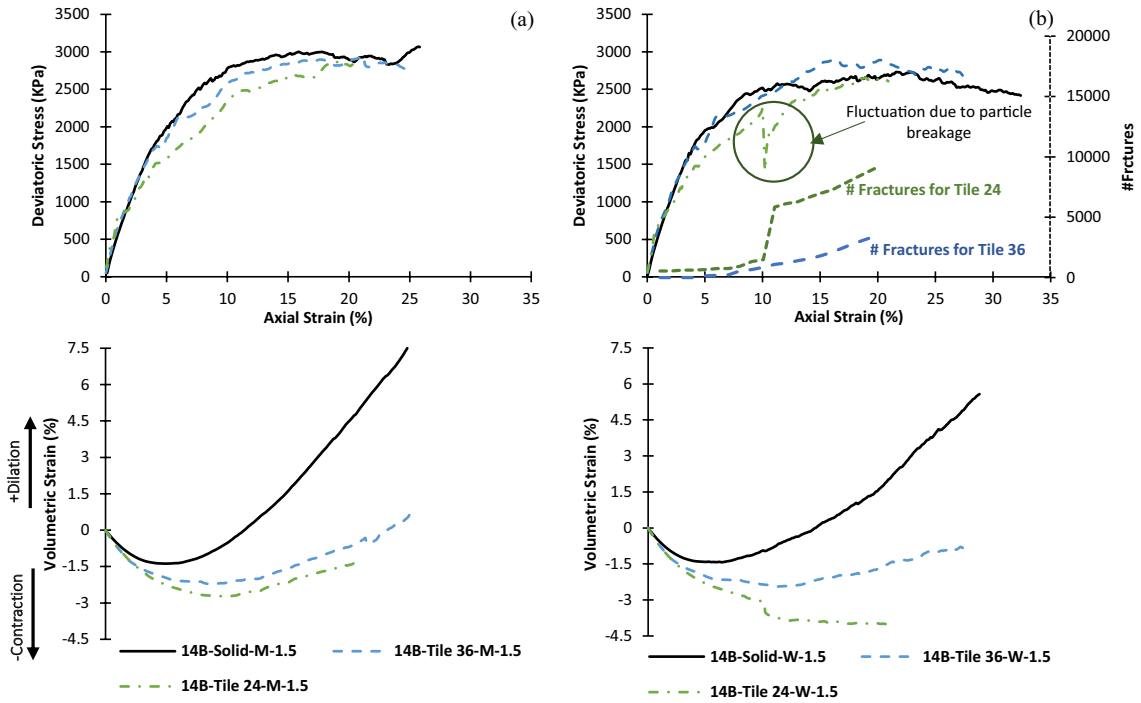

Fig. 7 Tiles resolution effect on the stress–strain behaviour of 14B particles assemblies under 1.5 MPa confining stress for **a**) Medium and **b**) Weak particles

and flexible membranes. Further elaboration on this topic is provided in the next section, where the mobilized friction angle as a strength factor is discussed. Considering the mobilised deviatoric stress, this effect is particularly evident at lower confining stresses (1.5 MPa), where fewer particles are broken. The increased angularity of 4B particles causes greater dilation at lower axial strains. However, as axial strain increases, the breakage phenomenon overcomes the effect of angularity, resulting in lower dilation at the residual stage compared to 14B particles. This trend is more obvious for the strong (Fig. 11(a)) and medium (Fig. 11(c)) particles confined under 1.5 MPa stress.

In the case of 14B particles, the emergence of finer daughter sub-particles following the replacement of the mother particle under critical stress conditions leads to greater compaction of the assembly which can be seen through Fig. 9, particularly for weak particles (Fig. 11(c)). This phenomenon is particularly exaggerated at high confining stresses of 2 MPa (where breakage is higher than 1.5 MPa) and in the case of weak particles where the majority of mother particles are broken, as shown in Fig. 11(c).

The Diagram of particle displacement confined under 2MPa stress using TBFM with H_{part} of 20 and V_{sec} equal to 36 (labelled as "Tile 36" in the triaxial models' results) for the assembly of Medium particles for two different shapes of 14B and 4B are shown in Fig. 12. The critical daughter particles are also highlighted in Fig. 12. It is apparent that these fractured particles are clustered in two regions: (i) the shear band zones, and (ii) the areas where the particle displacements are markedly distinct, resulting in increased relative displacement and higher applied stresses on the particles in these regions.

As previously noted, the 14B particles possess smaller sub-particles compared to the 4B particles. This finer subdivision results in a cushioning effect when the particles are crushed during the shearing stage of the triaxial test modelling, leading to a more densely packed sample. As a result, the displacement of the particles within the assembly of 14B particles is generally higher than that in the assembly of 4B particles (Fig. 12(a)). The accumulated effect of this phenomenon at high axial strains results in higher dilation and lower mobilised deviatoric stress or shear strength of the assembly in comparison to the assembly of 4B particles as demonstrated in Fig. 11(b).

Moreover, the assembly of 14B particles is in the bulging condition which stems from the smoother stress distribution due to the rearrangement of daughter sub-particles. It is worth noting that the cushioning effect and redistribution of stress resulted in fewer number of broken particles. On the other hand, the assembly of the 4B particles shows two

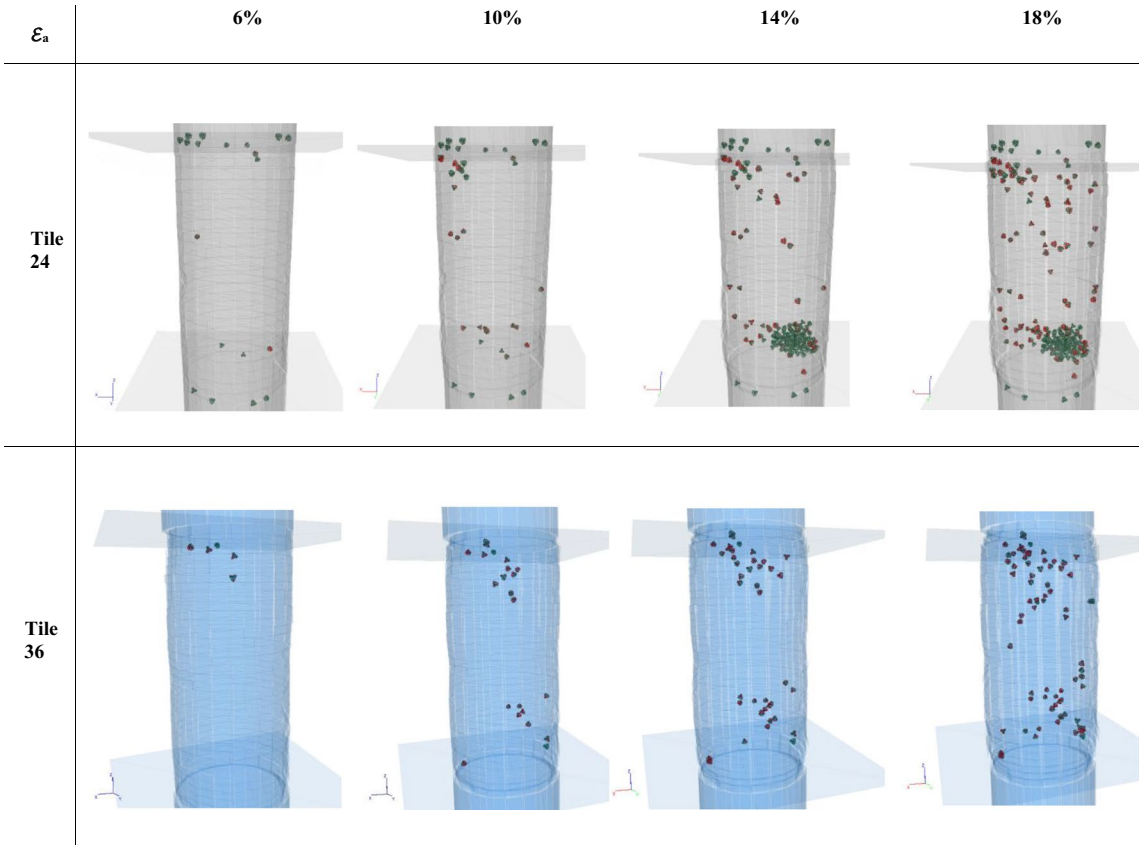

Fig. 8 Fractures development by increase in axial strain. (Broken bonds under tension are depicted in red, while those under shear are shown in green. Breakage events are recorded and illustrated in their original occurrence location, remaining fixed as walls and grains shift)

distinct shear blocks sliding against each other, as shown in Fig. 12(b). Also, the number of broken particles in this assembly is higher than in the 14B particles' assembly which is due to (i) the lower intrinsic strength of bigger sub-particles, and (ii) bigger daughter sub-particles of this particle shape and concentrated stress on the critical particles.

The angularity and shape of particles substantially affect the extent and distribution of breakage. This effect primarily relies on the characteristic strength of the particles, the applied confining stress, and the boundary conditions. Figure 13 presents a comparative analysis of normalised fracture events and breakage phenomena for the two different particle shapes 14B and 4B under varying confining stresses of 1.5 and 2 MPa, considering both semi-rigid (Solid) and flexible (Tile 36) boundary conditions. It should be noted that in Fig. 13, the number of fracture events is normalised using the number of bonds between each mother particle for 14B and 4B shapes. Upon examining Fig. 13(a) to (c), it becomes evident that the ratio of particle breakage between 4 and 14B particles decreases when transitioning from a semi-rigid to a flexible membrane, as well as when reducing the confining stress. In addition to the magnitude and frequency of fractures, it is noteworthy that breakage events are unevenly distributed in different directions for 4B Particles.

In the case of weak and highly breakable particles, particularly when a solid membrane is employed, the fracture rosette diagrams for both 14B and 4B particles exhibit a similar pattern, as depicted in Fig. 13(d). However, the difference becomes more pronounced when a flexible membrane is used, as evident in Fig. 13 (e). Therefore, when a relatively large number of breakage events occur within the assemblies, the fracture distribution will be nearly identical for both 4B and 14B particle shapes under the flexible membrane conditions of Tile 36. However, the magnitude of fractures notably decreases for the more angular shape of 4B particles. Interestingly, reducing the confining stress to 1.5 MPa alters this pattern, as illustrated in Fig. 13(f). Under relatively low confining stress of 1.5 MPa, and particularly in the case of weak particles, the 4B particles exhibit not only a higher fracture magnitude but also greater fluctuations in the distribution of breakage events.

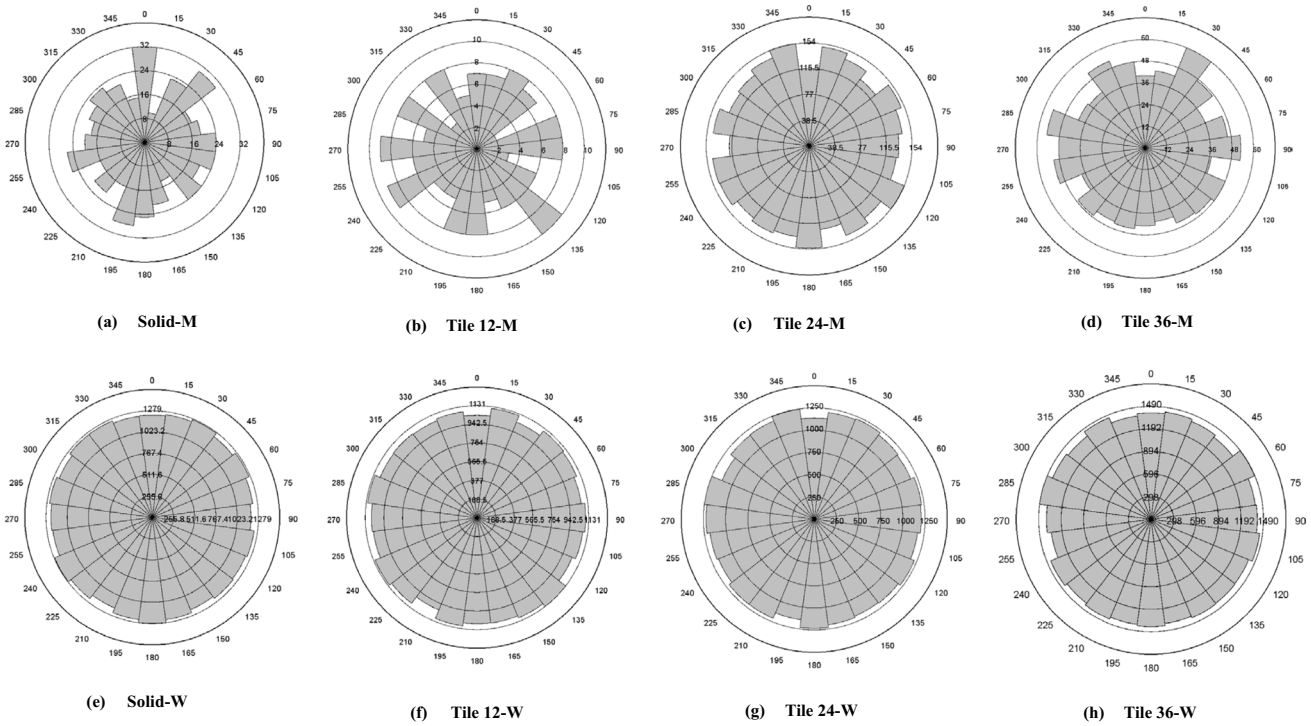

Fig. 9 Fracture rosette plots for Medium (a to d) and Weak (e to h) particles confined within different membranes under 2 MPa confining stress and at 25% axial shearing strain. (Note: the graphs are not to scale, and the quantity of fractures varies in each graph)

The variation in the mean effective stress, along with the deviatoric stress, during the shearing stage of a triaxial test plays a crucial role in altering the mobilized friction angle within an assembly. This parameter holds significant importance in the engineering design of rockfill structures. Figure 14 showcases the maximum friction angle obtained for different configurations, including varying resolutions of a flexible membrane, distinct particle shapes, and different confining stresses. Analysing Fig. 14(a), it is apparent that the maximum friction angle is mobilized at higher mean effective stresses for both strong and medium particles confined within a solid membrane. However, the difference in the mobilized friction angle between highly breakable weak particles and strong particles is substantially larger when compared to the difference observed in the case of a flexible membrane, which is illustrated with arrows in Fig. 14(a) (red arrow shows the difference for the solid membrane and the blue one illustrates the difference for Tile 36). Therefore, the flexibility of the membrane has a considerable effect on the maximum friction angle of breakable particles. Moreover, as the resolution of TBFM increases and the membrane becomes more flexible, the disparity between the maximum friction angles of strong and weak particles diminishes.

The effect of particle shape (4B versus 14 B) under different confining stresses (1,5 and 2.0 MPa) for solid and flexible membranes is depicted in Fig. 14(b). As anticipated, the maximum friction angle of 4B particles surpasses that of the 14B particles which exhibit a more rounded shape. Furthermore, this higher maximum friction angle is mobilized at higher mean effective stresses. Interestingly, the difference in the maximum mobilized friction angle between weak and strong particles is less pronounced for 4B shape under 2 MPa stress compared to the difference observed for the 14B shape, regardless of whether a flexible or solid membrane is utilised. This phenomenon can be attributed to the cushioning effect provided by broken particles, which facilitates stress redistribution among the relatively angular 4B particles. Consequently, finer broken daughter particles enhance the efficiency of stress redistribution among the angular 4B particles, resulting in a higher maximum mobilized friction angle for weak particles.

Notably, the flexible membrane intensifies this effect, leading to a slightly higher mobilized friction angle for Tile 36 compared to the solid membrane under 2 MPa confinement. These effects and phenomena become less prominent and diminish for relatively lower confining stresses of 1.5

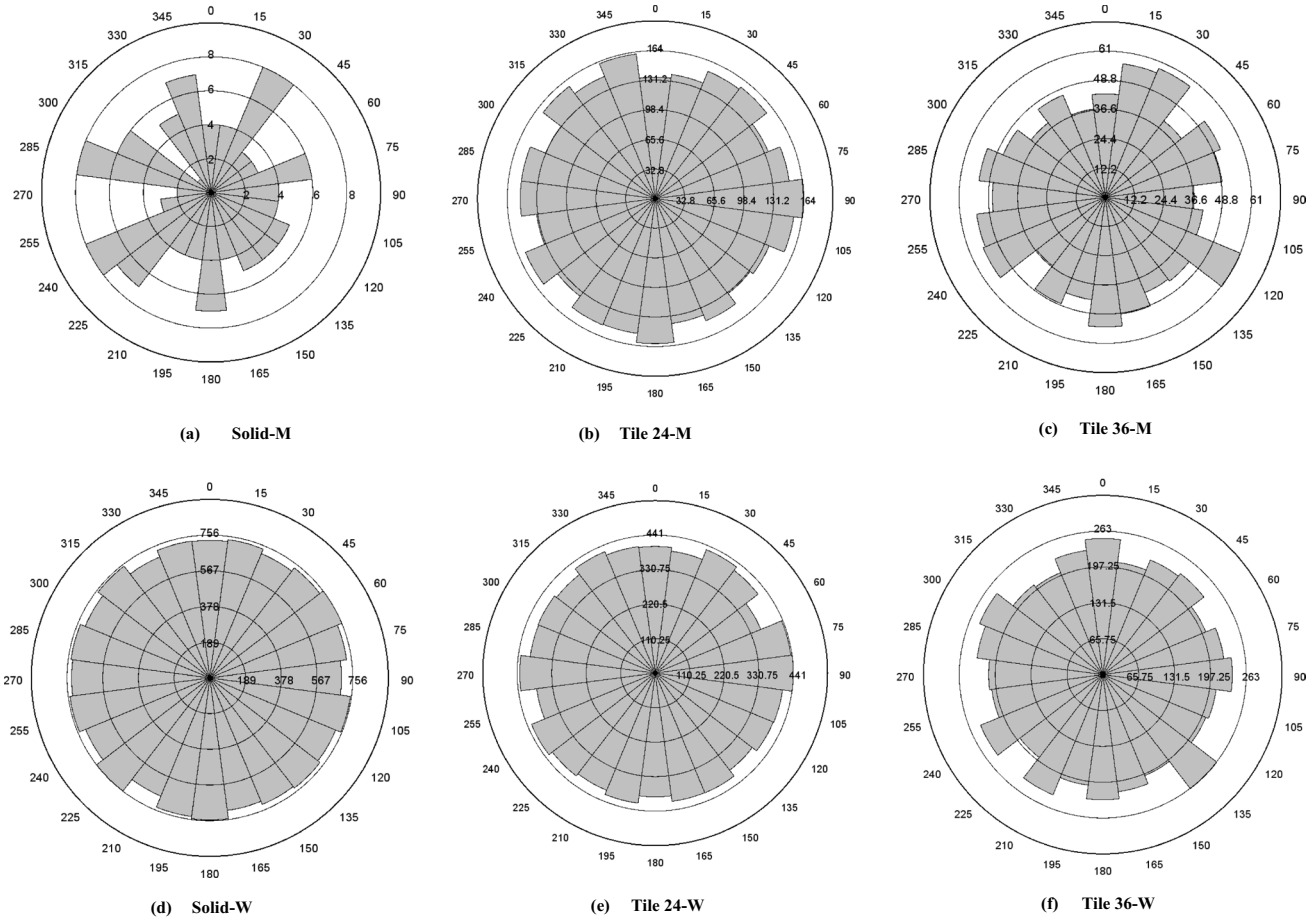

Fig. 10 Fracture rosette plots for Medium (a to c) and Weak (d to f) particles confined within different membranes under 1.5 MPa confining stress and at 25% axial shearing strain (Note: the graphs are not to scale, and the quantity of fractures varies in each graph)

MPa. However, for all three characteristic strengths, the maximum friction angle of 4B particles remains higher than that of the 14B particles, although the difference in mobilized friction angles for particles with different strengths becomes negligible.

As previously discussed, the utilisation of a flexible boundary condition and tile-based membrane primarily influences the volumetric behaviour of rockfill assemblies. Building upon the earlier section and the analysis of the mobilized friction angle, which is predominantly a stress-related parameter, it becomes apparent that stress-related parameters for the non-breakable strong particles are relatively consistent between the semi-rigid and flexible membrane conditions. However, a distinct difference can be observed in terms of void ratio and volumetric conditions for various resolutions and flexibility of membrane, even for non-breakable particles, as depicted in Fig. 15(a) and (b) where change in minimum normalised void ratio (Y axis) is shown against mean effective stress (X-axis).

The capacity of semi-rigid membranes to capture changes in volumetric strain and void ratio is limited due to the uniform displacement of each solid segment from bottom to top of the cell. Consequently, the difference in minimum normalized void ratios for the solid membrane is less pronounced compared to the flexible membranes. In the case of the solid membrane, medium and strong particles exhibit nearly identical normalized void ratios, whereas weak particles are compacted to lower normalized void ratios. Although the difference in normalized void ratio between medium and strong particles becomes less significant for flexible membranes, the difference in the amount related to the weak particles becomes more prominent with an increase in tile resolution, as demonstrated in Fig. 15(a).

Furthermore, it is evident that the minimum normalised void ratio is captured in higher mean effective stresses for the flexible membranes in comparison to the solid one, which may be attributed to a more favourable condition for particle rearrangement. Observing Fig. 15(b) clarifies that

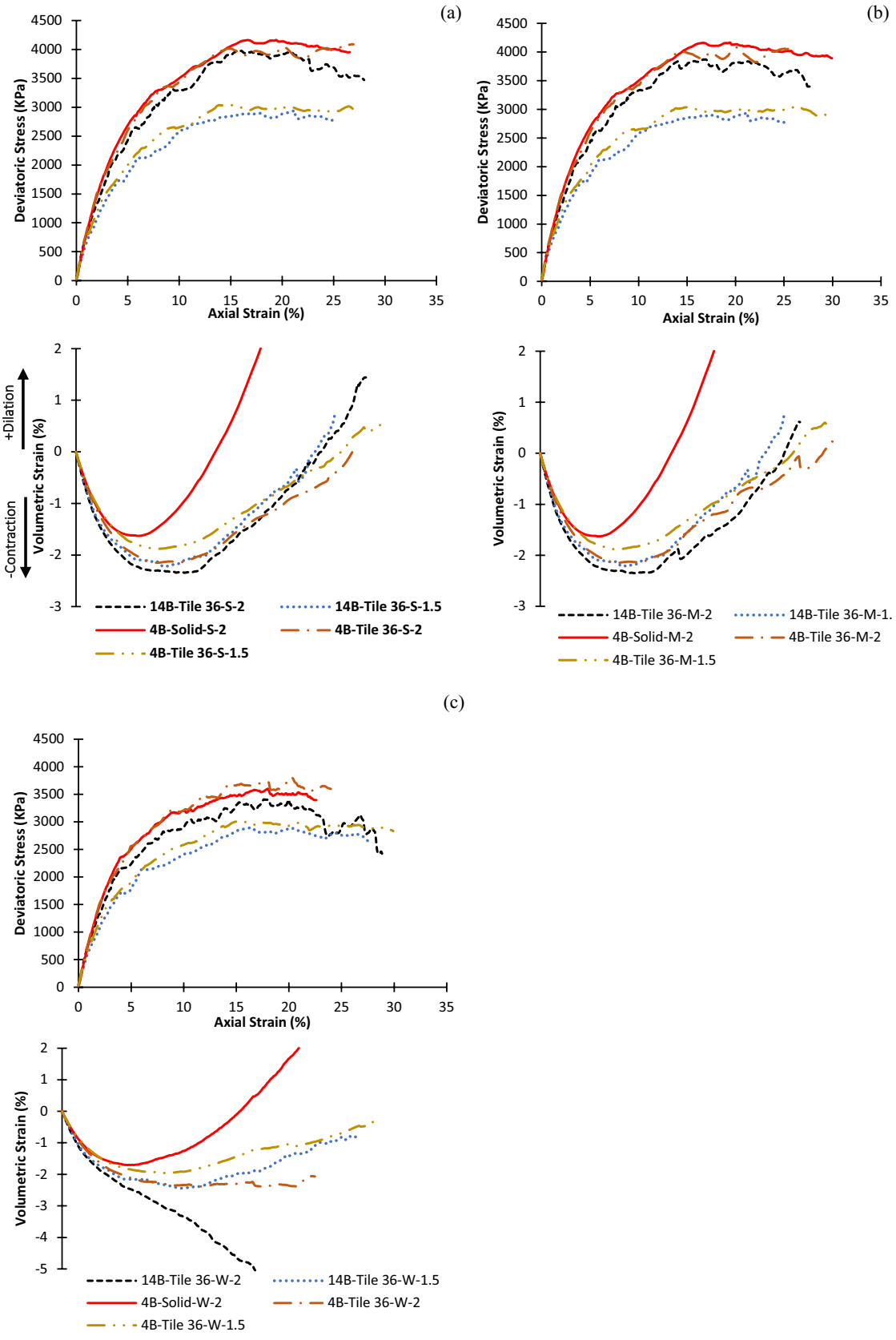

Fig. 11 Triaxial numerical test results for different particle shapes composed of 14 Balls and 4 Balls for a) Strong, b) Medium, and c) Weak particles

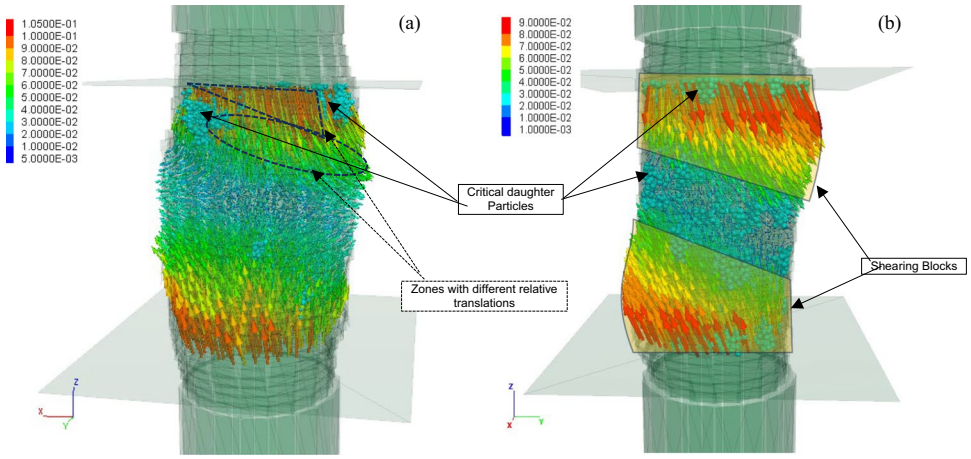

Fig. 12 Particle displacement for assembly of the Medium particles confined under 2 MPa confining stress and at 25% shearing axial strain for particle shape of **a**) 14B and b) 4B

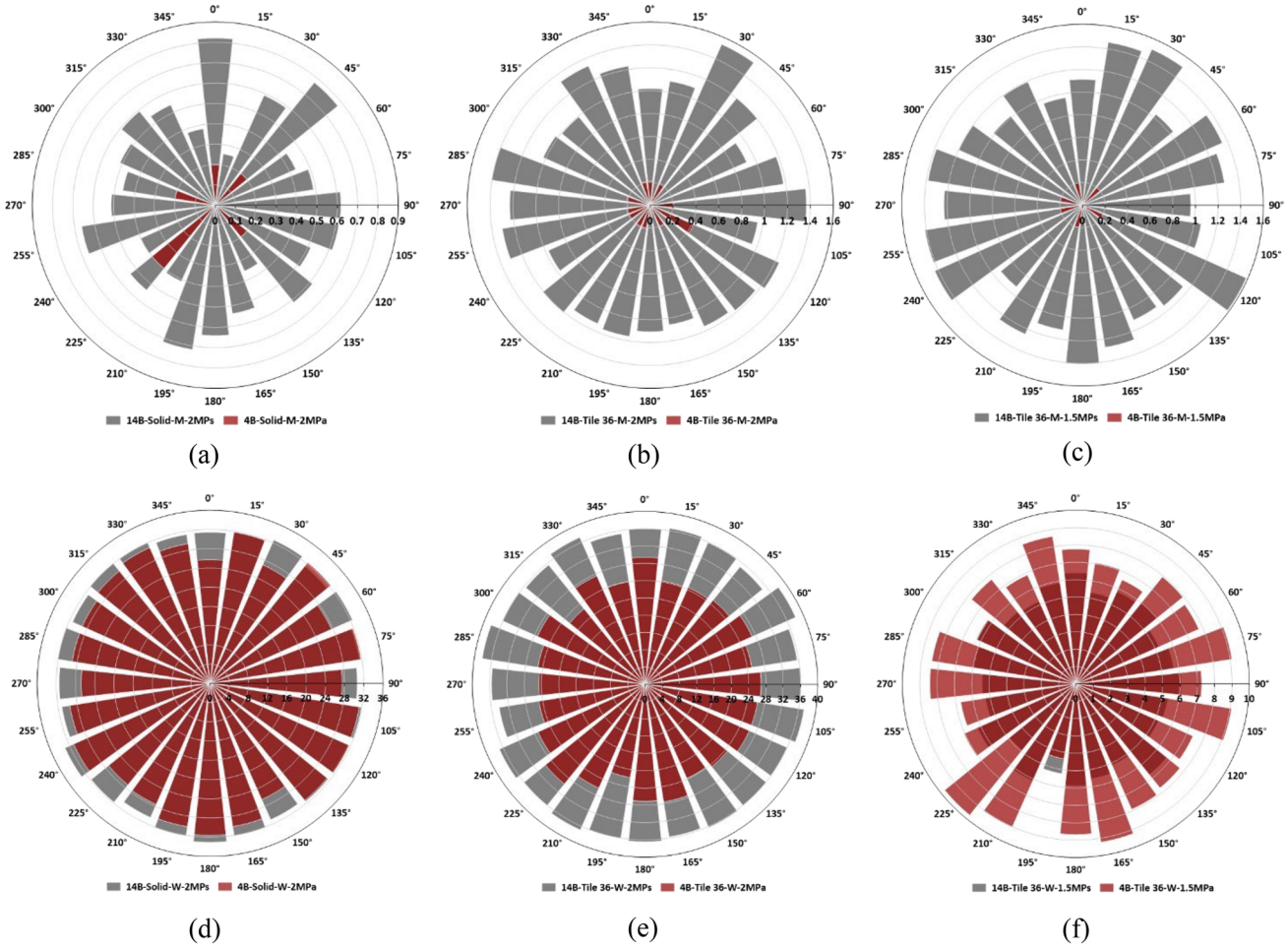

Fig. 13 Comparison of normalised fracture rosette diagrams for particle shapes of 14B (grey diagrams) and 4B (red diagrams) under different confining stresses of 1.5 and 2 MPa in semi-rigid (Solid) and flexible (Tile 36) boundary conditions: **a**-**c**) Medium particles; **d**-**f**) Weak particles

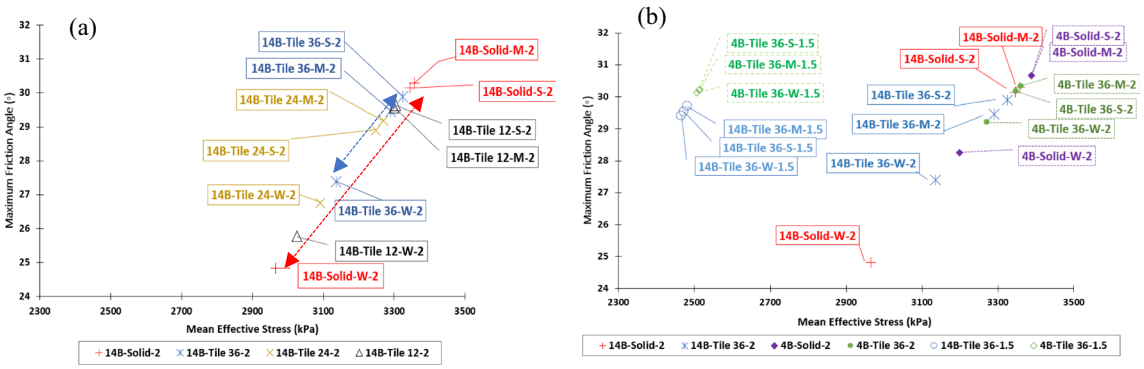

Fig. 14 Variation of maximum mobilised friction angle and corresponding mean effective stress; a) 14B particles under 2 MPa confining stress and for different resolutions of TBFM, b) comparison of 14B and 4B particle shapes under 1.5 and 2 MPa confining stresses

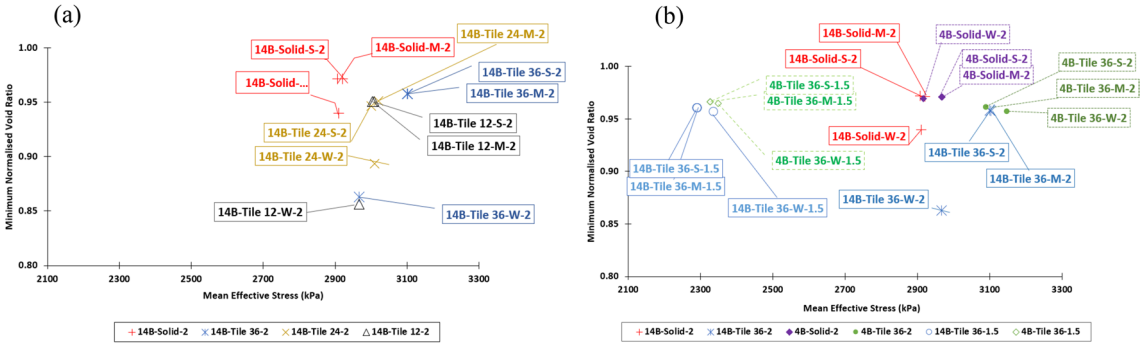

Fig. 15 Minimum normalised void ratios versus corresponding mean effective stresses; a) 14B particles under 2 MPa confining stress and for different resolution of TBFM, b) comparison of 14B and 4B particle shapes under 1.5 and 2 MPa confining stresses

the increased angularity of 4B particles leads to a higher minimum normalized void ratio for weak particles, which is also captured in higher mean effective stresses. Although the difference between 4 and 14B particles becomes negligible under relatively lower confining stress of 1.5 MPa, 4B particles still reach higher minimum normalized void ratios at higher mean effective stresses.

To improve the understanding of changes in volume and void ratio, Fig. 16 presents an illustration of the organization of non-breakable mother particles alongside the replaced critical daughter particles. Within this figure, the distribution of non-breakable mother particles (depicted as red clumps) and critical breakable daughter particles (represented by green clusters) are shown. These particles pertain to the category of Weak and Medium strong particles under a 2 MPa confining stress that are enclosed within a solid and flexible membrane consisting of 36 rows of tiles. The difference in void areas between assemblies of weak and medium particles is more pronounced and evident for the solid membrane (Fig. 16(a) and (b)) compared to the difference observed in the void area of the Tile36 flexible membrane (Fig. 16(c) and (d)). When examining assemblies of highly breakable particles (Weak particles) at the end of the shearing stage, confined within both solid (Fig. 14(a)) and flexible (Fig. 14(c)) membranes, a distinct difference in stress distribution due to boundary conditions emerges. In the case of the solid or semi-rigid membrane, the broken particles and shear band zones tend to concentrate predominantly near the rigid cylindrical wall, with zones primarily oriented horizontally. Conversely, within the flexible membrane, where the influence of membrane solidity is reduced, the broken particles and shear band zones develop at the middle sample, extending from the top to the bottom and exhibiting a diagonal orientation.

5 Discussion and conclusions

In this paper, the effect of particle shape, confining stress, breakage phenomenon, and boundary condition on the mechanical behaviour of rockfill particles is studied using the Modified Particle Replacement Method (MPRM) previously introduced by the authors as the breakage simulation algorithm. Furthermore, the effect of a flexible membrane in the triaxial

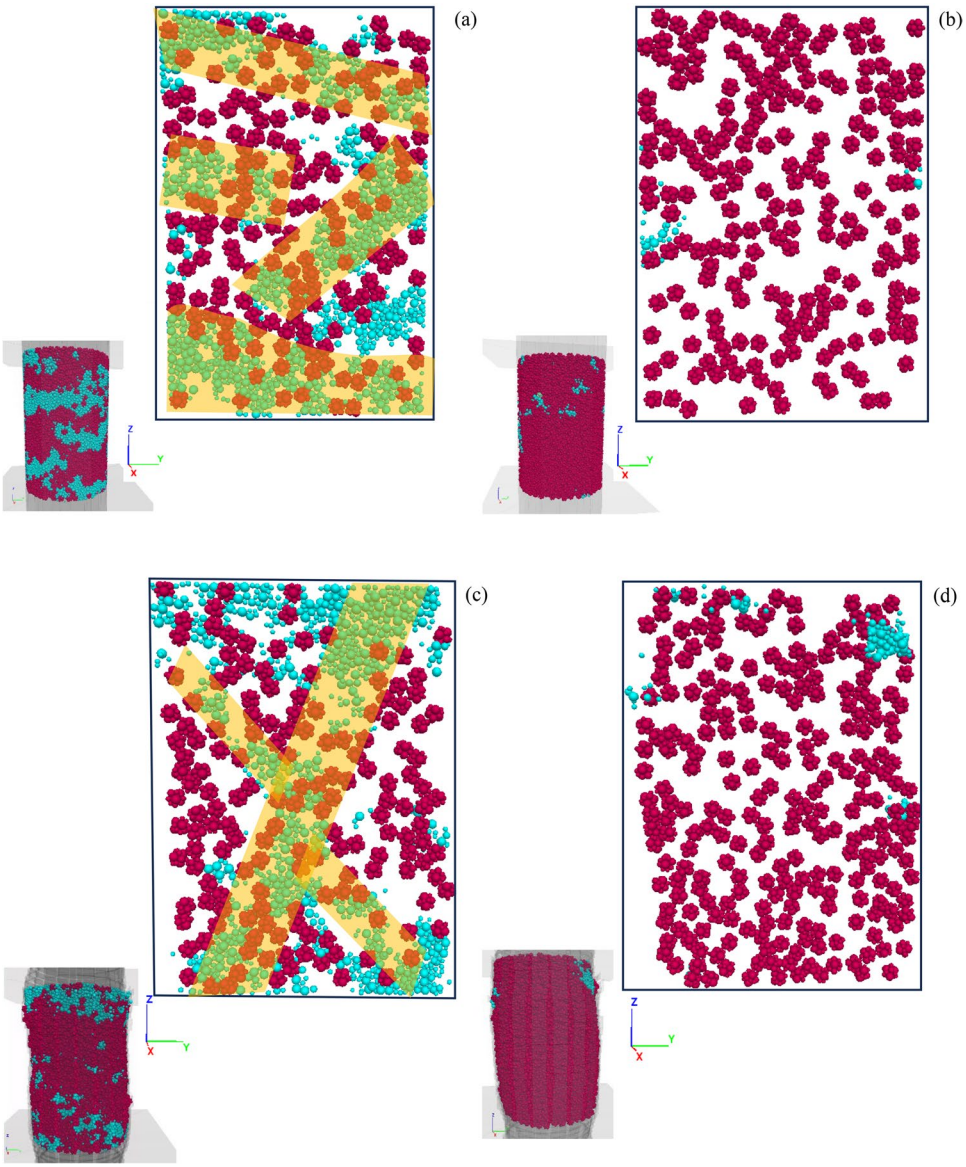

Fig. 16 Arrangement of non-breakable mother particles (depicted in red clumps) and critical breakable daughter particles (illustrated in green clusters) under 2 MPa confining stress, within a platen cross-section (X–Y plane) at the middle of the samples and at the end of shearing stage (25% axial strain). This depiction concerns 14B particles and encompasses a) Weak particles with Solid membrane, b) Medium particles with Solid membrane, c) Weak particles with Tile36 flexible membrane, and d) Medium particles with Tile36 flexible membrane

test modelling on the particle breakage and mechanical behaviour is investigated through the Tile-Based Flexible Membrane (TBFM) theory in which independent small rigid rectangular walls form a cylindrical deformable membrane that can freely move inward and outward to achieve the target confining stress.

In this study, two different particle shapes composed of 14 and 4 balls have been employed in the numerical simulations. For the parametric study of the numerical model, a series of triaxial tests have been conducted on a sample of 30 (diameter) × 70 cm (height) using semi-rigid (solid) and flexible membranes with $H_{part} = 20$, and $V_{sec} = 12$, 24, and 36. The number and size of the tiles were adjusted to balance computational demand and membrane deformability. It was found that for a minimum tile dimension larger than the smallest particle size, the area difference between tile-based and circular cross-sections was below 1% for $H_{part} > 20$. Thus, the study limited the number of tiles in each ring to 20 and investigated different numbers of rings (V_{sec}) to achieve the desired flexibility.

The deviatoric stress in the samples with solid membranes is slightly higher than that in the samples with flexible membranes for assemblies of Strong and Medium particles. However, the results showed that using a flexible membrane leads to higher peak and residual mobilized strengths compared to a solid (semi-rigid) membrane, particularly for Weak particles prone to breakage. The rearrangement of particles facilitated by the flexible membrane contributed to the generation of higher strength. Additionally, increasing the resolution of the tiles and the flexibility of the membrane resulted in a transition from a dense to a loose behaviour in the stress–strain response of the sample, with a continuous decrease in strength within the residual zone.

The flexible membrane mainly affects volumetric behaviour. This becomes more pronounced for weak particles, where a large number of breakages are observed. Samples confined by a solid membrane displayed a more dilative behaviour, while those tested with a flexible membrane exhibited reduced dilation. Increasing the number of tile rings and resolution reversed the reduction in dilation and shifted the volumetric strains towards positive values. Furthermore, the use of a flexible membrane captures changes in volumetric strain and void ratio more effectively than a solid membrane. Weak particles tend to have lower normalized void ratios compared to medium and strong particles, and this difference becomes more pronounced with an increase in tile resolution and flexibility of the membrane.

The fracture distribution analysis showed that higher membrane resolution led to a smoother distribution of fractures in all directions for medium particles. In the case of weak particles, an increased number of tile rows resulted in an escalated occurrence of fractures in all directions. The confining stress also influenced fracture distribution, with higher confining stresses generally leading to a smoother distribution of fractures.

The variation in mean effective stress and deviatoric stress during the shearing stage of a triaxial test has a significant impact on the mobilized friction angle within an assembly, both are crucial considerations for the engineering design of rockfill structures. The flexibility of the membrane used in the test setup plays a considerable role in determining the maximum friction angle, particularly for breakable particles. As the resolution of the test setup increases and the membrane becomes more flexible, the difference in maximum friction angles between strong and weak particles diminishes.

The particle shape had a significant impact on the mechanical behaviour of the assemblies. The angular particles exhibit higher maximum friction angle values. The cushioning effect provided by broken particles enhances stress redistribution among angular particles, leading to higher maximum friction angles for weak particles. The flexible membrane further intensifies this effect. Particle shape 4B, with higher angularity, exhibited higher strength compared to particle shape 14B due to its higher angularity, especially at lower confining stresses where fewer particles were broken. However, as axial strain increased, the breakage phenomenon overcame the effect of angularity, resulting in lower dilation at the residual stage compared to particle shape 14B. In other words, the assembly of particles with higher angularity shows a higher strength and greater dilation at lower axial strains. This effect is particularly evident at lower confining stresses.

The Diagram of particle displacement using coupled MPRM and TBFM shows that the fractured particles are clustered in two regions: (i) the shear band zones, and (ii) the areas where the particle displacements are markedly distinct, resulting in increased relative displacement. The finer daughter sub-particles result in a cushioning effect when the particles are crushed during the shearing stage, leading to a more densely packed sample and higher dilation and lower shear strength.

Moreover, the assembly of 14B particles is in the bulging condition which stems from the smoother stress distribution due to the rearrangement of finer daughter sub-particles. On the other hand, the assembly of the 4B particles shows two distinct shear blocks sliding against each other. Also, the number of broken particles in this assembly is higher than that in the 14B particles assembly which is due to; (i) the lower intrinsic strength of bigger pebbles, and (ii) the bigger daughter sub-particles of this particle shape and concentrated stress on the critical particles.

Supplementary Information The online version contains supplementary material available at https://doi.org/10.1007/s10035-024-01441-3.

Acknowledgements The first author acknowledges The University of Melbourne for support provided through Melbourne Research Scholarship. The authors would like to acknowledge ATC Williams for initiating the research idea and support throughout the studies and ITASCA group for their willingness to share information and provide support through ITASCA Educational Partnership (IEP) program. Also, the authors acknowledge Dr. Amirhassan Mehdizadeh for his invaluable technical support.

Funding Open Access funding enabled and organized by CAUL and its Member Institutions

Data Availability All data, models, or code generated or used during the study are available from the corresponding author by request.

Declarations

Competing interests The authors declare the following financial interests/personal relationships which may be considered as potential competing interests:

References

1. Leps, T.M.: Review of shearing strength of rockfill. Journal of Soil Mechanics & Foundations Division **96**(4), 1159–1170 (1970)
2. Marsal, R.J.: Large-scale testing of rockfill materials. Journal of the Soil Mechanics and Foundations Division **93**(2), 27–43 (1967)

3. Alonso, E.E., Tapias, M., Gili, J.: Scale effects in rockfill behaviour. Géotechnique Letters **2**(3), 155–160 (2012)
4. Frossard, É., et al.: Rockfill shear strength evaluation: a rational method based on size effects. Géotechnique **62**(5), 415–427 (2012)
5. Jiang, M., Xie, Y., Liu, J.: DEM Investigation on the scale effect on macroscopic and microscopic mechanical behavior of rockfills. In: proceedings of Geoshanghai 2018 international conference: fundamentals of soil behaviours, pp. 835–839. Springer, Singapore (2018)
6. Marsal, R.J.: Mechanical properties of rockfill. Publication of, Wiley (John) and Sons, Incorporated (1973)
7. Lade, P.V., Yamamuro, J.A., Bopp, P.A.: Significance of particle crushing in granular materials. Journal of Geotechnical Engineering **122**(4), 309–316 (1996)
8. Yang, G., Yan, X., Nimbalkar, S., Xu, J.: Effect of particle shape and confining pressure on breakage and deformation of artificial rockfill. Int. J. Geosynth. Ground Eng. **5**, 1–10 (2019)
9. Tapias, M., Alonso, E.E., Gili, J.A.: A particle model for rockfill behaviour. Géotech. **65**(12), 975–994 (2015)
10 Oldecop, L.A.: and E. Alonso Pérez de Agreda, Theoretical investigation of the time-dependent behaviour of rockfill (2007)
11. Einav, I.: Breakage mechanics—Part I: Theory. J. Mech. Phys. Solids **55**(6), 1274–1297 (2007)
12. Varadarajan, A., et al.: Testing and modeling two rockfill materials. Journal of geotechnical and geoenvironmental engineering **129**(3), 206–218 (2003)
13. Guo, Y., Chi, S., Mi, X., Yan, S.: Experimental investigation of statistical characteristics of elastic mechanical parameters and strength indexes of rockfill particles. Granular Matter. **25**(2), 30 (2023)
14. Zhao, B., et al.: An investigation of single sand particle fracture using X-ray micro-tomography. Géotechnique **65**(8), 625–641 (2015)
15. Oldecop, L.A.: and E. A model for rockill compressibility, Alonso Pérez de Agreda (2001)
16. Yu, F.W.: Particle breakage and the critical state of sands. Géotechnique **67**(8), 713–719 (2017)
17. Xiao, Y., Liu, H., Chen, Y., Jiang, J.: Strength and deformation of rockfill material based on large-scale triaxial compression tests. II: influence of particle breakage. J. Geotech. Geoenviron. Eng. **140**(12), 04014071 (2014)
18. Jia, Y., Xu, B., Chi, S., Xiang, B., Zhou, Y.: Research on the particle breakage of rockfill materials during triaxial tests. Int. J. Geomech. **17**(10), 04017085 (2017)
19. Nie, Z., Zhu, Y., Wang, X., Gong, J.: Investigating the effects of fourier-based particle shape on the shear behaviors of rockfill material via DEM. Granular Matter. **21**, 1–15 (2019)
20. Bagherzadeh-Khalkhali, A., Mirghasemi, A.A., Mohammadi, S.: Micromechanics of breakage in sharp-edge particles using combined DEM and FEM. Particuology **6**(5), 347–361 (2008)
21. Raisianzadeh, J., Mohammadi, S., Mirghasemi, A.A.: Micromechanical study of particle breakage in 2D angular rockfill media using combined DEM and XFEM. Granular Matter. **21**(3), 1–27 (2019)
22. Xu, M., Hong, J., Song, E.: DEM study on the macro- and micro-responses of granular materials subjected to creep and stress relaxation. Comput. Geotech. **102**, 111–124 (2018)
23. Ciantia, M.O., et al.: DEM modelling of cone penetration tests in a double-porosity crushable granular material. Comput. Geotech. **73**, 109–127 (2016)
24. Bruchmüller, J., et al.: Modelling discrete fragmentation of brittle particles. Powder Technol. **208**(3), 731–739 (2011)
25. Lobo-Guerrero, S., Vallejo, L.: DEM analysis of crushing around driven piles in granular materials. Géotechnique **55**(8), 617–623 (2005)
26. Russell, A.R., Muir Wood, D.: Point load tests and strength measurements for brittle spheres. International Journal of Rock Mechanics and Mining Sciences **46**(2), 272–280 (2009)
27. de Bono, J., McDowell, G.: Particle breakage criteria in discrete-element modelling. Géotechnique **66**(12), 1014–1027 (2016)
28. Zhou, W., et al.: Discrete element modeling of particle breakage considering different fragment replacement modes. Powder Technol. **360**, 312–323 (2020)
29. Asadi, R., Disfani, M.M., Ghahreman-Nejad, B.: A new modified replacement method for discrete element modelling of rockfill material. Comput. Geotech. **168**, 106168 (2024)
30. Cheung, L.Y.G., O'Sullivan, C., Coop, M.R.: Discrete element method simulations of analogue reservoir sandstones. Int. J. Rock Mech. Min. Sci. **63**, 93–103 (2013)
31. Zhang, P., et al.: Experimental simulation and a reliable calibration method of rockfill microscopic parameters by considering flexible boundary. Powder Technol. **396**, 279–290 (2022)
32. de Bono, J., McDowell, G., Wanatowski, D.: Discrete element modelling of a flexible membrane for triaxial testing of granular material at high pressures. Géotechnique Letters **2**(4), 199–203 (2012)
33. Ma, G., et al.: Combined FEM/DEM modeling of triaxial compression tests for rockfills with polyhedral particles. Int. J. Geomech. **14**(4), 04014014 (2013)
34 Liu, D., Yang, J., Dong, B.: Discrete element analysis of the influence of compaction quality on mechanical properties of rockfill materials. Computers and Geotechnics **151**, 104358 (2022)
35. Zhao, X., Evans, T.M.: Discrete simulations of laboratory loading conditions. Int. J. Geomech. **9**(4), 169–178 (2009)
36. Khoubani, A., Evans, T.M.: An efficient flexible membrane boundary condition for DEM simulation of axisymmetric element tests. Int. J. Numer. Anal. Meth. Geomech. **42**(4), 694–715 (2018)
37. Cheng, Y., Nakata, Y., Bolton, M.D.: Discrete element simulation of crushable soil. Geotechnique **53**(7), 633–641 (2003)
38. Ciantia, M.O., et al.: An approach to enhance efficiency of DEM modelling of soils with crushable grains. Géotechnique **65**(2), 91–110 (2015)
39 Russell, A.R., Muir Wood, D., Kikumoto, M.: Crushing of particles in idealised granular assemblies. Journal of the Mechanics and Physics of Solids **57**(8), 1293–1313 (2009)
40. Weibull, W.: A statistical distribution function of wide applicability. J. Appl. Mech. **18**(3), 293–297 (1951)
41. McDowell, G.R., De Bono, J.P.: On the micro mechanics of one-dimensional normal compression. Géotechnique **63**(11), 895–908 (2013)
42. Lees, G.: A new method for determining the angularity of particles. Sedimentology **3**(1), 2–21 (1964)
43. Khonji, A., Bagherzadeh-Khalkhali, A., Aghaei-Araei, A.: Experimental investigation of rockfill particle breakage under large-scale triaxial tests using five different breakage factors. Powder Technol. **363**, 473–487 (2020)
44. Jia, Y., Xu, B., Chi, S., Xiang, B., Xiao, D., Zhou, Y.: Particle Breakage of Rockfill Material during Triaxial Tests under Complex Stress Paths. Int. J. Geomech. **19**(12), 04019124 (2019)
45. Ma, G., Zhou, W., Chang, X.-L.: Modeling the particle breakage of rockfill materials with the cohesive crack model. Comput. Geotech. **61**, 132–143 (2014)
46. Guo, W.-L., et al.: Estimations of Three Characteristic Stress Ratios for Rockfill Material Considering Particle Breakage. Acta Mech. Solida Sin. **32**(2), 215–229 (2019)